Raymo, M.E., Jansen, E., Blum, P., and Herbert, T.D. (Eds.), 1999
Proceedings of the Ocean Drilling Program, Scientific Results, Vol. 162

10. AGE MODELS FOR GLACIAL FAN DEPOSITS OFF EAST GREENLAND AND SVALBARD (SITES 986 AND 987)[1]

J.E.T. Channell,[2] Morten Smelror,[3] Eystein Jansen,[4] Sean M. Higgins,[5] B. Lehman,[6] Tor Eidvin,[7] and A. Solheim[8]

ABSTRACT

Cores recovered at Sites 986 and 987 comprise glacial fan sedimentation associated with the Svalbard-Barents Sea and Greenland Ice Sheets, respectively. At Site 986, the top 150 m and the basal 250 m yielded interpretable magnetic stratigraphies. The record from the intervening 550 m is compromised by drilling-related core deformation, poor recovery, and numerous debris flows. The uppermost 150 m appears to record the Brunhes/Matuyama boundary and the Jaramillo Subchron. The base of the drilled section (at ~950 meters below seafloor [mbsf]) is interpreted to lie within the Matuyama Chron (age <2.58 Ma) with an apparent normal polarity interval in the ~730–750 mbsf interval. Dinoflagellate cyst biostratigraphy and Sr isotopic ratios are consistent with a Matuyama age for the base of the drilled section and with the normal polarity interval as the Olduvai Subchron. On the other hand, the last occurrence of *Neogloboquadrina atlantica* (sinistral) and the last common occurrence of the warm-dwelling *Globigerina bulloides* at 647–650 mbsf in Hole 986D indicate an age for this level of ~2.3 Ma, inconsistent with the designation of the Olduvai Subchron in the ~730–750 mbsf interval. If the age at 647–650 mbsf in Hole 986D is taken as 2.3 Ma and the base of the hole lies within the Matuyama Chron, then the sedimentation rate in the basal 300 m of the cored section averages 1 m/k.y.

At Site 987, the magnetic stratigraphy is fairly unambiguous throughout the section and yields an age of 7.5 Ma (Chron 4n) for the base of the drilled section. The paucity of calcareous and siliceous microfossils precludes biostratigraphic corroboration of the magnetostratigraphic interpretation, although dinoflagellate cysts provide general support, particularly at the base of the section. The age model indicates relatively low sedimentation rates (~5 cm/k.y.) at the base of the section with rates at least four to five times greater during intervals of debris flows at ~5–4.6 and ~2.6 Ma.

INTRODUCTION

The principal objective at Sites 986 and 987 was to determine the age of glacial fan deposits that record the Neogene history of the Svalbard-Barents Sea and Greenland Ice Sheets, respectively. Shipboard paleontology at both sites indicated that siliceous and calcareous microfossils would provide little in the way of biostratigraphic age constraints. Shore-based work on dinoflagellates at both sites (see Smelror, Chap. 6, this volume) has provided a biostratigraphy. The dinoflagellate datums, however, are too poorly correlated with other biozonations (and to the polarity time scale) to ratify the details of the magnetostratigraphic interpretations at Sites 986 and 987.

Site 986 (77.34°N, 9.08°E) is located on the eastern flank of the Knipovich Ridge off the western Svalbard margin (Fig. 1). Basement depth at this site was estimated from seismic stratigraphy to be 1170 meters below seafloor (mbsf). The maximum penetration (at Hole 986D) was 964.6 mbsf (Shipboard Scientific Party, 1996a). Seismic Reflector R7 corresponds to the boundary between lithostratigraphic Subunits IVA and IVB at 897.3 mbsf. This reflector marks the base of the glacial sediments and can be traced to the glacial fan depocenter off Bjørnøya (Bear Island) (Fig. 1), where it lies at ~3500 mbsf (Fiedler and Faleide, 1996). Age control on this and other seismic reflectors recovered at Site 986 will provide important constraints on the age of the glacial sediments of the entire margin and hence illuminate the history of the Svalbard-Barents Sea Ice Sheet.

Site 987 (70.50°N, 17.94°W) is located on Anomaly 5 (10 Ma) oceanic crust at the mouth of the Scoresby Sund, a major conduit for glacial detritus from the Greenland Ice Sheet (Fig. 1). As much as 6 km of mid-Miocene to recent sediments have been deposited in a bowl-shaped depression of the basement at the mouth of the Scoresby Sund (Larsen, 1990). At Site 987, to the northeast of the depocenter (Fig. 1), the thickness of the glacial fan is considerably reduced. However, the major seismic reflectors (R1–R5) can be traced from the depocenter to the site, providing a chronology that is applicable to the depositional system as a whole. Although the basement was not reached at Site 987, the maximum penetration (860 mbsf) is comparable to the depth to basement estimated from seismic stratigraphy.

MAGNETIC STRATIGRAPHY

Methods

Archive halves of all core sections were measured on board ship using the cryogenic pass-through magnetometer. The high rate of core recovery at these sites required that cores be processed promptly; therefore, stepwise alternating field (AF) demagnetization was generally not feasible during the cruise. Most core sections were measured aboard ship at a single demagnetization step (generally 25 mT); the choice of peak field was based on stepwise demagnetization of a few core sections and a handful of discrete samples.

The shipboard pass-through magnetometer data are "noisy," particularly at Site 986. There are several likely sources of this "noise": (1) magnetic overprints derived from the drill string, (2) drilling- and dropstone-related core deformation, (3) chaotic remanence directions

[1]Raymo, M.E., Jansen, E., Blum, P., and Herbert, T.D. (Eds.), 1999. *Proc. ODP, Sci. Results,* 162: College Station, TX (Ocean Drilling Program).
[2]241 Williamson Hall, Department of Geology, University of Florida, Gainesville, Florida 32611, U.S.A. jetc@nervm.nerdc.ufl.edu
[3]The Norwegian University of Science and Technology, Museum of Natural History and Archaeology, Erling Skakkes gt. 47, N-7004 Trondheim, Norway.
[4]Department of Geology, University of Bergen, Allégaten 41, N-5007 Bergen, Norway.
[5]Lamont-Doherty Earth Observatory of Columbia University, Palisades, NY 10964, U.S.A.
[6]Laboratoire des Sciences du Climat et de l'Environnement, CNRS-CEA, Avenue de la Terrasse, 91198 Gif-sur-Yvette, France.
[7]Norwegian Petroleum Directorate, P.O. Box 600, N-4001 Stavanger, Norway.
[8]Norwegian Polar Institute, P.O. Box 5072, Mororstua, N-0301 Oslo, Norway.

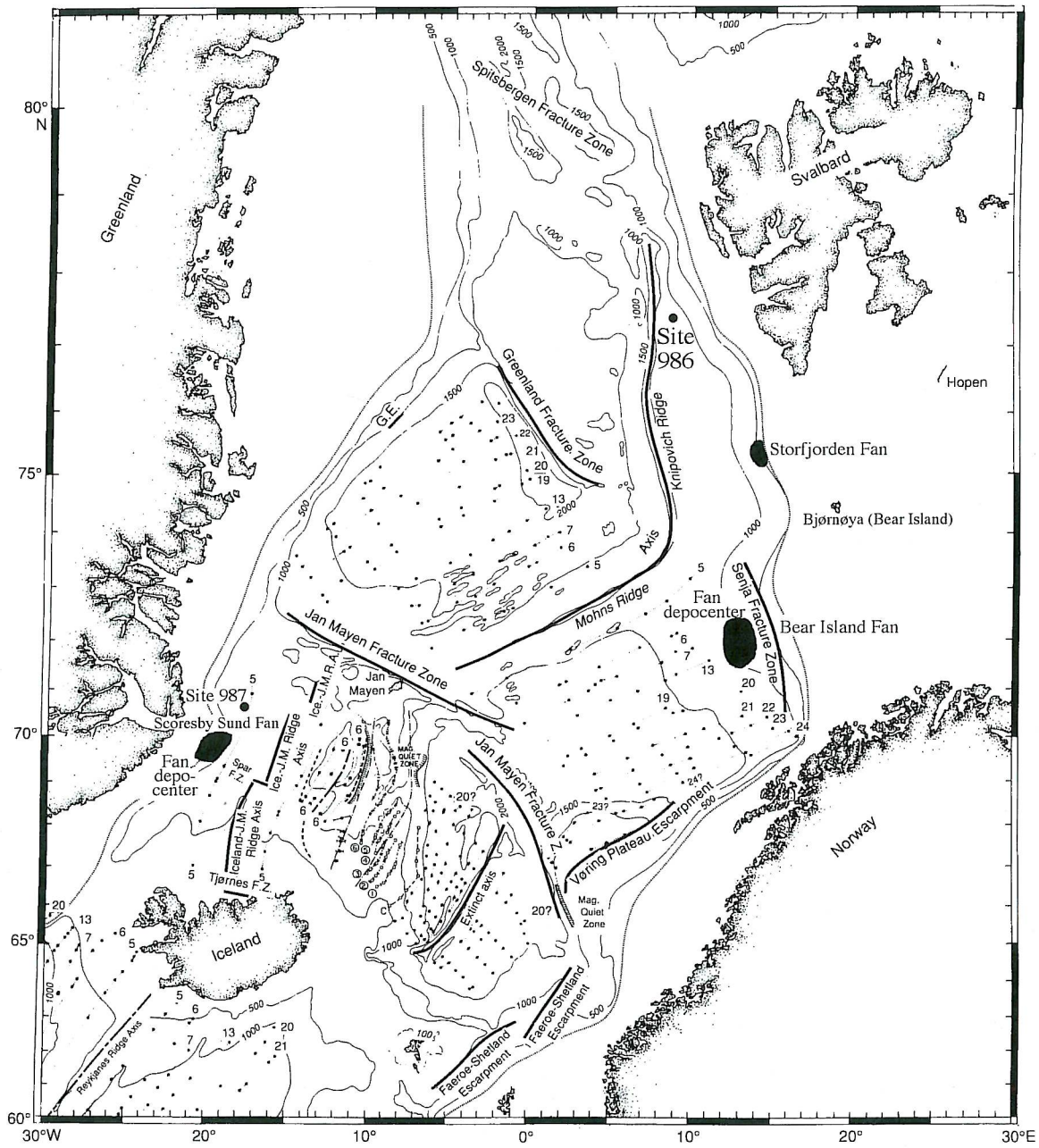

Figure 1. Location map for Sites 986 and 987 indicating oceanic magnetic anomaly numbers (after Talwani and Eldholm, 1977) and the position of the Neogene depocenters associated with the glacial fans emanating from the Greenland and Svalbard–Barents Sea Ice Sheets.

within debris flows, and (4) diagenetic (secondary) remanence acquisition. Drilling-related deformation and debris flows can be avoided by discrete sampling, and a complete demagnetization sequence can be carried out on discrete samples to "ground truth" the shipboard magnetic stratigraphy.

Discrete samples were collected during the cruise in the standard 7-cm^3 plastic boxes and measured at laboratories at Gif-sur-Yvette and at the University of Florida. Natural remanent magnetization was measured before demagnetization and during stepwise alternating field demagnetization using a peak field increment of 5 mT in the 5- to 70-mT range, or until the magnetization intensity fell below magnetometer noise level. Orthogonal projections of AF demagnetization data indicated that a characteristic magnetization component could usually be resolved at peak fields >~20 mT. A lower coercivity component was observed in most samples, particularly those with a reverse polarity characteristic component. The low coercivity component is oriented steeply downcore and is probably a viscous and/or "stirred" remanent magnetization imposed by the drill string and/or the bottom-hole assembly. The characteristic (higher coercivity) magnetization component was picked by eye from orthogonal projections, and its direction was computed using the standard least-squares technique (Kirschvink, 1980).

Site 986

Resistivity wireline logs at Holes 986C and 986D indicate the presence of numerous debris flows, which appear as highs in resistivity (Fig. 2A). The output of the shipboard pass-through magnetometer is incoherent in the 160–700 mbsf interval because of (1) the abundance of debris flows, (2) ubiquitous drilling-related core defor-

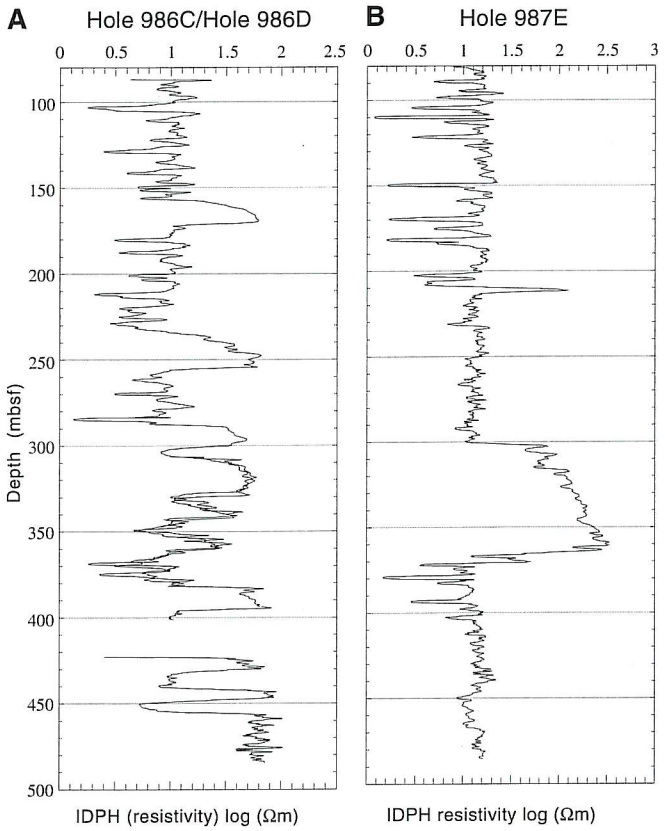

Figure 2. IDPH (phasor deep-induction resistivity) wireline logs for **(A)** Holes 986C and 986D and **(B)** Hole 987E.

mation enhanced by the high concentration of dropstones, and (3) poor recovery.

Above 160 mbsf, recovery is relatively high and the concentration of dropstones relatively low. Discrete samples from this interval indicate that a well-defined characteristic magnetization component can be defined after demagnetization at peak fields of ~20 mT (Fig. 3). A steep downward low-coercivity magnetization component is apparent and attributable to the drill string. In the 160–270 mbsf interval, the drill-string magnetic overprint is more pronounced and is beginning to overwhelm the characteristic magnetization (Fig. 3).

The Brunhes/Matuyama boundary at Hole 986C is not defined by the shipboard pass-through data (Fig. 4). It is, however, apparent in the component inclination data derived from discrete samples and occurs at ~130 mbsf (Fig. 4). The top of a normal polarity zone at ~150 mbsf may be correlative to the Jaramillo Subchron. A thick debris flow in the 158–173 mbsf interval (Fig. 2A) interrupts the inclination record. The sediments immediately below the debris flow indicate negative inclinations (reverse polarity). Below 200 mbsf, poor recovery and core deformation curtail the record (Fig. 4).

The upper part of the section at Hole 986D was drilled but not cored. Coring was begun at 387.8 mbsf, but poor recovery, abundant dropstones, and drilling-related deformation precluded resolution of a magnetic stratigraphy in the upper ~300 m of the cored section. Only below ~700 mbsf do the sediments at Hole 986D become sufficiently indurated to resist the rigors of rotary core barrel drilling. Magnetization components are poorly defined in Hole 986D below 715 mbsf (Fig. 5). However, normal and reverse magnetization components can be resolved from discrete samples, and the distribution of component inclinations generally ratifies the shipboard pass-through data (Fig. 6; Table 1). Below 900 mbsf, recovery is poor. Nonetheless, with the exception of a well-defined normal polarity interval in the 735–755 mbsf interval, the 700–900 mbsf interval has mainly reverse polarity. We tentatively interpret this normal polarity interval as the Olduvai Subchron and consider that the base of the hole lies within the Matuyama Chron.

The geological high-resolution magnetic tool (GHMT) wireline logs at Hole 986C provided some corroboration for the magnetostratigraphic interpretation at the top of the section. Following Pozzi et al. (1993), the polarity interpretation of the GHMT data is based on the nature of the correlation of magnetic susceptibility and magnetic remanence variations recorded by the tool. Positive correlations of susceptibility and remanence imply normal polarity, and negative correlations imply reverse polarity. The correlations are assessed in a number of sampling windows, increasing from ~1 to ~25 m from left to right in Figure 7. The Brunhes/Matuyama boundary appears to be defined at ~130 mbsf and the top of the Jaramillo at ~150 mbsf (Fig. 7), close to their positions in the core (Fig. 4). The base of the Jaramillo is not defined either in the core or in the log due to the occurrence of a debris flow in the 158–173 mbsf interval.

Site 987

The shipboard pass-through magnetometer data from the upper part of Holes 987A, 987B, and 987D, derived after demagnetization of peak fields of 25 mT, is noisy (Fig. 8), probably because of a combination of drilling-related core deformation and inadequate removal of the drill-string magnetic overprint. Discrete samples collected at Hole 987D often indicate well-defined magnetization components (Fig. 9). A steeply inclined drill-string magnetization is removed at peak demagnetization fields of ~20 mT. This overprint is particularly apparent in reverse polarity samples. Although the demagnetization behavior of discrete samples indicates that the magnetization components are well defined (Fig. 9), component inclinations for Hole 987D are moderately scattered (Fig. 8). The discrete sample data generally ratify the shipboard pass-through magnetometer data. The Brunhes/Matuyama boundary and the Jaramillo and Olduvai Subchrons appear to be well defined (Fig. 8; Table 2).

Downsection, below 360 mbsf, discrete samples from Hole 987E yielded well-defined magnetization components (Figs. 10, 11). Component inclinations from discrete samples are generally consistent with the shipboard pass-through data at Hole 987E (Figs. 12, 13), where the record spans the interval from the base of the Matuyama Chron at 360 mbsf (Fig. 12) to Chron 4n at 850 mbsf (Fig. 13).

The GHMT log at Hole 987E provides support for the magnetostratigraphic interpretation in the 95-300 mbsf interval (Fig. 14). The base of the Jaramillo, the Olduvai Subchron, and the Reunion events appear to be recorded in the log. The base of the logged section lies at the top of a thick debris flow (Fig. 2B). Comparison of the GHMT data with the core magnetic stratigraphy (Fig. 8) indicates consistency in the location of the base of the Jaramillo, and of the boundaries of the Olduvai and Reunion Subchrons.

CHRONOLOGY

Site 986

The lack of biostratigraphic constraints at Site 986, and the fact that the acquisition of a chronostratigraphy was the major objective at this site, has meant that much emphasis has been placed on the magnetic stratigraphy. Although the data quality is poor, the following conclusions can be drawn. The Brunhes/Matuyama boundary and the top of the Jaramillo can be placed at ~130 and ~150 mbsf, respectively (Fig. 4; Table 1). The highest occurrence of *Pseudoemiliania lacunosa* is at 120 mbsf in Hole 986A, which implies that this level is older than 0.46 Ma (Shipboard Scientific Party, 1996a). At the base of the section in the 700–950 mbsf interval, the predominance of negative inclinations is consistent with the interval as part of the Matuyama Chron. A well-defined normal polarity interval in the 735–755 mbsf interval (Fig. 6) may correlate with the Olduvai Subchron, although this designation is inconsistent with the presence of the fora-

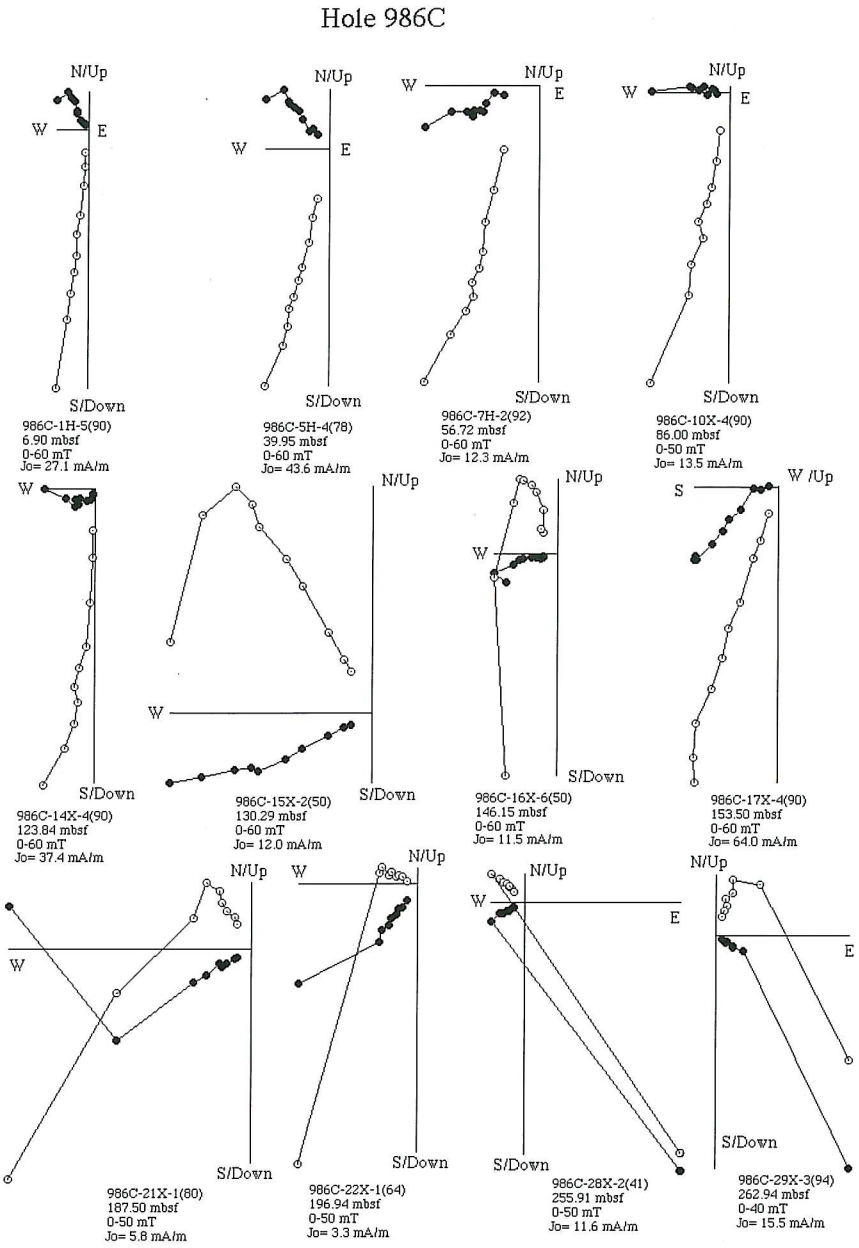

Figure 3. Orthogonal projection of AF demagnetization data from discrete samples in the 0–263 mbsf interval of Hole 986C. Open and solid symbols indicate projection on the vertical and horizontal planes, respectively.

minifer *Neogloboquadrina atlantica* (sinistral). Shipboard studies indicated the sporadic presence of *N. atlantica* (sinistral) between 707 and 842 mbsf in Hole 986D (Shipboard Scientific Party, 1996a). Subsequent shore-based studies suggested that this foraminifer occurs throughout the 648–955 mbsf interval in Hole 986D (Eidvin and Nagy, Chap. 1, this volume). On the Vøring Plateau, the last occurrence (LO) of *N. atlantica* (sinistral) occurs in the lower part of the Matuyama Chron at ~2.3 Ma (Spiegler and Jansen, 1989). A very similar age (2.3–2.35 Ma) has been calculated for this datum from Sites 981 and 982 in the North Atlantic (Channell and Lehman, Chap. 8, this volume), in agreement with the compilation of Berggren et al. (1995a). If the base of the recovered section lies within the Matuyama Chron, as implied by the paleomagnetic data, and the LO of *N. atlantica* (sinistral) is at 2.3 Ma at this site, then the entire 648–955 mbsf interval was apparently deposited in the 2.3–2.6 Ma interval with a mean sedimentation rate of ~1 m/k.y. The warm-dwelling *Globigerina bulloides* is common in Pliocene sediments older than 2.4 Ma on the Vøring Plateau (Spiegler and Jansen, 1989). The last common occurrence of *G. bulloides* at 649 mbsf in Hole 986D (Eidvin and Nagy, Chap. 1, this volume) is consistent with the LO of *N. atlantica* and implies an age of ~2.3 Ma for this level.

Dinoflagellate cysts provide further chronostratigraphic constraints. Close to the base of Hole 986D, the last appearance datum (LAD) of *Selenopemphix brevispinosa* at 928.34 mbsf and the LAD of *Invertocysta lacrymosa* at 909.14 mbsf would be expected to lie close to the Matuyama/Gauss boundary at ~2.6 Ma, consistent with the base of the hole being within the Matuyama Chron. The acme of *Filisphaera filifera* occurs at 804.84 mbsf in Hole 986D (Fig. 15). The range of this species defines the PM2 dinoflagellate zone of Mudie (1989). The acme might be expected to lie in the Matuyama Chron below the Olduvai Subchron since the Olduvai is recorded in the 735–755 mbsf interval at Hole 986D (Fig. 6). The LAD of *Sumatradinium pliocenicum* at 564.44 mbsf and the LAD of *Amiculosphaera umbracula* at 333.53 mbsf would be expected to lie only just above the Olduvai Subchron in the 1.5–1.6 Ma interval. Toward the top of the section, the LAD of *Operculodinium israelianum* at

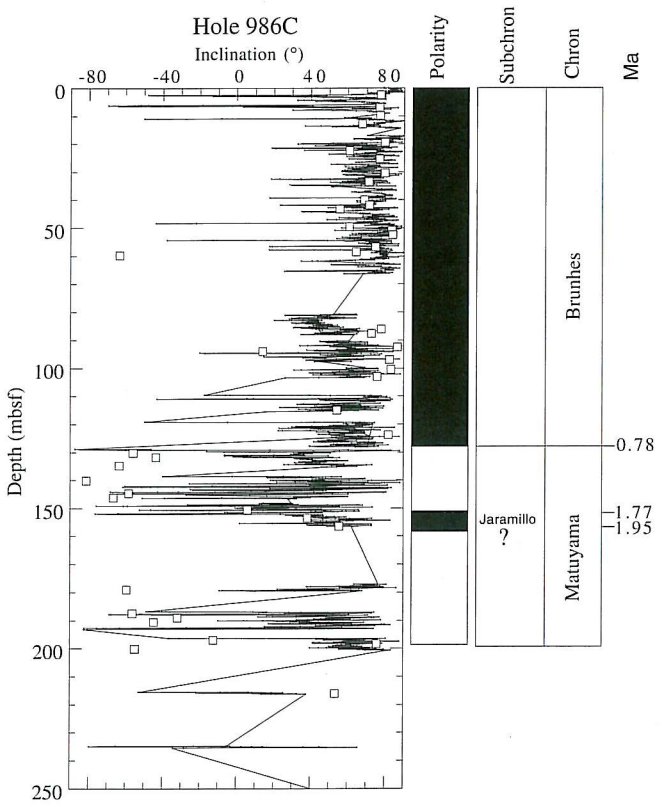

Figure 4. Shipboard (pass-through magnetometer) inclination data after AF demagnetization at peak fields of 25 mT for Hole 986C in the 0–250 mbsf interval. Open squares indicate component inclinations determined from discrete (7 cm^3) samples measured postcruise. Component directions computed from orthogonal projections of AF demagnetization data.

122.18 mbsf would probably lie close to the Brunhes/Matuyama boundary, consistent with the magnetic stratigraphy (Fig. 4). Similarly, the acme of *Operculodinium centrocarpum* at 66.04–58.04 mbsf, lying in the mid-Brunhes, is as expected. In summary, the dinoflagellate data are broadly consistent with the magnetostratigraphic interpretations.

Strontium isotope data derived from benthic and planktic foraminifera in the 715–820 mbsf interval from Hole 986D (Table 3; Fig. 15) indicate ages (derived using the regression formula from Hodell et al., 1991) consistent with this interval having been deposited in the Matuyama Chron near the Olduvai Subchron. $^{87}Sr/^{86}Sr$ values obtained from benthic and planktic foraminifers in the interval 668–892 mbsf vary between 0.709131 and 0.709067 (see Forsberg et al., Chap. 17, this volume). There is a pronounced scatter in the results that may result either from analytical problems such as contamination or from the effects of redeposition of older specimens. This translates to an age span of 3.5 to 1.3 Ma using the age relationship of Farrell et al. (1995) on the Berggren et al. (1995b) time scale. The fit used by Farrell et al. (1995) is very flat in the age interval 2.7–4 Ma, hence ages older than 2.6–2.7 Ma are very uncertain. Despite the scatter, the Sr data indicate that the 900–670 mbsf interval at Hole 986D is younger than ~2.6 Ma, which verifies the reverse polarity interval at the base of the hole as the Matuyama Chron.

As discussed above, the lowest of a series of seismic reflectors at the site (R7) is considered to coincide with the boundary between lithostratigraphic Units IVA and IVB (Shipboard Scientific Party, 1996a) at 897 mbsf in Hole 986D (Fig. 15). This reflector can be correlated with the Bear Island Neogene depocenter (Fig. 1), where it marks the base of the glacial sediment pile. Off Bear Island (Fig. 1), drill cores penetrated an unconformity that has been correlated with R7. Glassy volcaniclastic debris from just below the unconformity have yielded ^{40}Ar–^{39}Ar eruption ages of ~2.3 Ma (Mork and Duncan, 1993). These age data are consistent with the 897 mbsf level at Hole 986D (correlated with R7) being in the early part of the Matuyama Chron (Fig. 15).

Site 987

Shipboard paleontological studies provided no useful age constraints for the sediment sequence recovered at Site 987. Calcareous nannofossils are virtually absent below Core 162-987A-5H, and calcareous foraminifers are absent below Core 162-987A-11X. The sequence is apparently barren of diatoms, radiolarians, and siliceous flagellates.

At Site 987, shore-based study of dinoflagellate cysts (M. Smelror, unpubl. data) has provided the only means of checking the magnetostratigraphic interpretations. In the Norwegian-Greenland Sea, owing to the absence of more traditional biostratigraphic indicators, dinoflagellate cysts have proved to be useful for Cenozoic chronology. Mudie (1989) defined four dinoflagellate zones (PM4–PM1) for the late Miocene to Pleistocene interval from Leg 104 (Vøring Plateau) sediments. Based on Hole 907A and Site 909 (Leg 151), Poulsen et al. (1996) defined several Miocene dinoflagellate zones and subdivided the Pliocene–Pleistocene into four zones. Comparison of the two zonal schemes is hampered by the fact that only one datum (LAD of *Unipontidinum aquaeductum*) is common to the two schemes. The LAD of *U. aquaeductum* defines the PM3/PM4 boundary in Mudie (1989) and the Mio6/Pli1 boundary in Poulsen et al. (1996).

At 775.14 mbsf at Hole 987E (Fig. 16), the LAD of *Labrinthodinium truncatum* defines the Mio6/Pli1 boundary of Poulsen et al. (1996), which these authors correlate with the NN11/NN12 nannofossil zonal boundary. The 775.14 mbsf level at Hole 987E corresponds to Chron 3Bn (Fig. 13), whereas the NN11/NN12 boundary correlates with Chron 3r (see Berggren et al., 1995b). The discrepancy is significant (almost 2 m.y.); however, it is clear that the datum does not correlate with Chron 3r at Hole 987E. Therefore, we attribute the discrepancy to miscorrelation of the dinoflagellate event with the NN11/NN12 boundary.

The LAD of *Reticulatosphaera actinocoronata* at 562.24 mbsf in Hole 987E lies within the Gilbert Chron in Subchron 3n.3n (Fig. 12). This datum defines the Pli1/Pli2 boundary of Poulsen et al. (1996), which these authors believe correlates with the NN14/NN15 nannofossil zonal boundary. The NN14/NN15 boundary correlates with Chron 2Ar (see Berggren et al., 1995b). The discrepancy is ~1 m.y. and is again attributed to miscorrelation of the dinoflagellate and nannofossil zonal boundaries, as the magnetic stratigraphy is unequivocal in this interval. Further confusion has resulted because this same datum was observed at 113 mbsf in Hole 907A by Poulsen et al. (1996). This level in Hole 907A, however, is in Chron 5n, considerably older than the apparent age of the datum in Hole 987E.

The LAD of *Evittosphaerula*? sp. 2 at 767.04 mbsf in Hole 987E correlates with Chron 3Bn (Fig. 13). The same datum was observed at 94.54 mbsf in Hole 907A (Poulsen et al., 1996). This level in Hole 907A corresponds to Chron 3An (Channell et al., Chap. 9, this volume). The discrepancy in the LAD of *Evittosphaerula*? sp.2 in Holes 987E and 907A is relatively modest (~0.5 m.y.) compared to the discrepancies cited above.

The acme of *Filisphaera filifera* at 690.11 mbsf and the LAD of this species at 240.54 mbsf defines the PM2 zone of Mudie (1989) and its top, respectively. The age for the top of PM2 given by Mudie (1989) is 1.4 Ma; however, the 240.54 mbsf level in Hole 987E is considerably older, close to 2 Ma.

Discrepancies between published correlations/ages for dinoflagellate zones (Mudie, 1989; Poulsen et al., 1996) and their correlation at Site 987 (Fig. 16) stem, we believe, from the uncertainties in the correlation of dinoflagellate datums with the polarity time scale

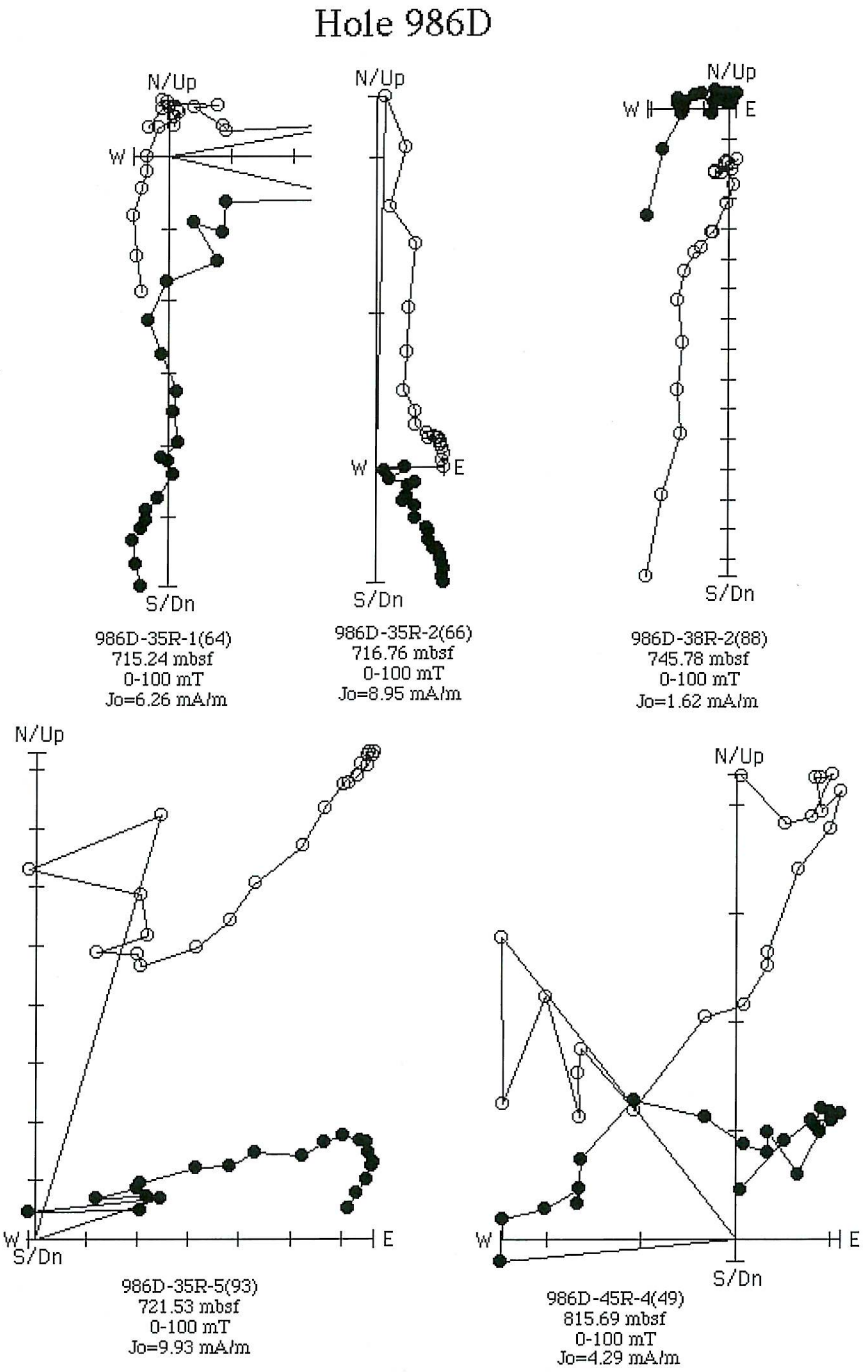

Figure 5. Orthogonal projection of AF demagnetization data from discrete samples in the 700–850 mbsf interval of Hole 986D. Open and solid symbols indicate projection on the vertical and horizontal planes, respectively.

and to nannofossil zones, not from errors in the proposed chronology for Site 987. Indeed, the Site 987 record provides the best available correlation of dinoflagellate events with the polarity time scale, and hence to absolute ages.

ACCUMULATION RATES AND HISTORY OF GLACIAL FAN DEPOSITION

Site 986

Extrapolation of sedimentation rates at the base of the section (Fig. 17) implies an age of ~2.6 Ma for the base of the drilled section at Site 986. Negative inclinations from the pass-through data at the base of Hole 986D (Fig. 6) indicate that the base of the section has an age within the Matuyama Chron (<2.58 Ma). The base of the drilled section lies ~50 m below the level correlated with Reflector R7 (Fig. 15), which is often used as the marker for the base of the Neogene glacial pile and can be traced southward to the depocenters of the western Barents Sea margin (Fiedler and Faleide, 1996; Faleide et al., 1996; Solheim et al., 1996). On the Vøring Plateau, the onset of large-scale Northern Hemisphere glaciation is dated at 2.75 Ma (Fronval and Jansen, 1996) and, therefore, coincides with the onset of Neogene glacial fan deposition off Svalbard.

The chronostratigraphy implies a distinct change in sedimentation rate between the Olduvai and Jaramillo Subchrons. Forsberg et al. (Chap. 17, this volume) interpreted lithostratigraphic Units IVA and

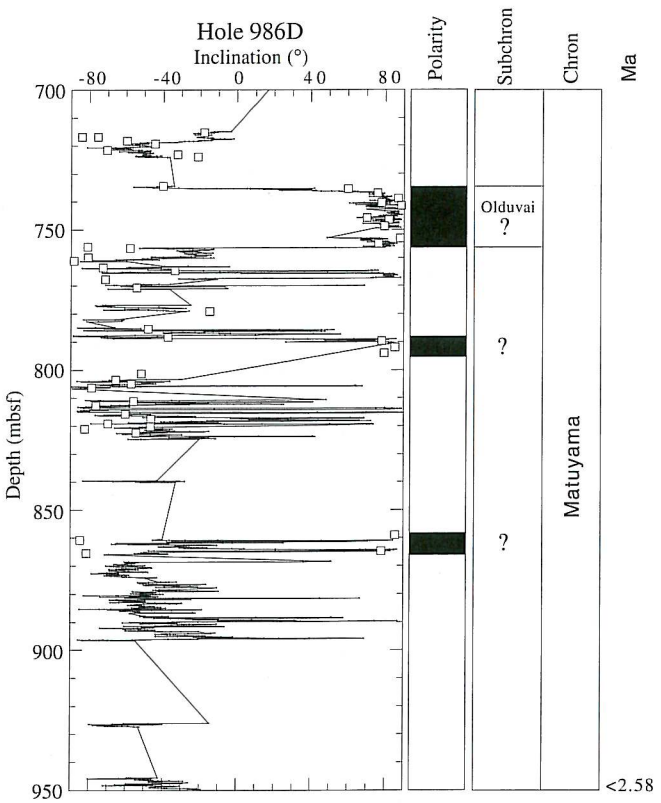

Figure 6. Shipboard (pass-through magnetometer) inclination data after AF demagnetization at peak fields of 25 mT for Hole 986D in the 700–950 mbsf interval. Open squares indicate component inclinations determined from discrete (7 cm^3) samples measured postcruise. Component directions computed from orthogonal projections of AF demagnetization data.

Table 1. Polarity chron boundaries at Site 986.

Event	Age (Ma)	Hole	Depth (mbsf)	Depth (mcd)
Brunhes/Matuyama	0.78	986C	127	133
Top, Jaramillo	0.99	986C	148	152
Top, Olduvai??	1.77	986D	735	735
Base, Olduvai??	1.95	986D	756	756
Reunion??	2.14	986D	792	792

III (seismic Unit SV-VII (Fig. 15) as sandy, silty debris flows with interbedded hemipelagic sediments. They documented an increased ratio of debris flows to hemipelagic sediments in the upper two-thirds of lithostratigraphic Unit III. Sedimentation rates probably increased gradually through Unit III with a large increase at the base of Unit II at 561 mbsf (seismic Reflector R6) as deposition was increasingly dominated by debris flows.

At ~1 Ma, the sedimentation rate at Site 986 appears to have slowed as debris flows diminished toward the top of lithologic Unit II (Fig. 17). Sedimentation rates during the Brunhes Chron averaged ~174 m/m.y. in contrast to sedimentation rates three or four times higher in the lower part of Unit II (Fig. 15). This change in sedimentation rate coincides with seismic Reflector R4, above which Andersen et al. (1994) noted a lateral shift in depocenters adjacent to Svalbard. This change seems to coincide with the middle Pleistocene climate shift at ~0.9 Ma (Berger and Jansen, 1994). Forsberg et al. (Chap. 17, this volume) noted a marked change in the mineralogy of sediments recovered near Reflector R5 (350–360 mbsf). They related

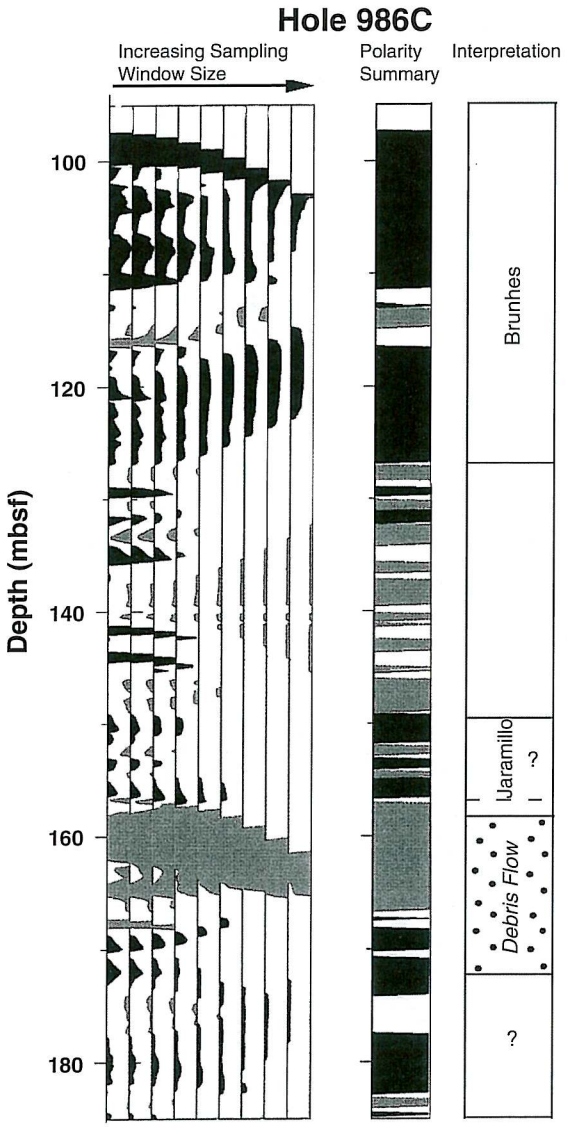

Figure 7. GHMT wireline logs at Hole 986C. Positive correlations of susceptibility and remanence imply normal polarities (black), and negative correlations imply reverse polarity (gray). The correlations were assessed in a number of sampling windows, increasing from ~1 to ~25 m from left to right. Only windows with lengths from 1.5 to ~12 m were used to create the polarity summary column based on a minimum correlation coefficient of 0.5.

this to a change in provenance from the Barents Sea to Svalbard in response to the submergence of a previously emergent Barents Sea platform. By interpolation between paleomagnetic datums (Fig. 15), this transformation may have occurred sometime between 1.5 and 1.0 Ma.

Site 987

The base of the drilled section at Site 987 is dated magnetostratigraphically at ~7.5 Ma (Fig. 16). On the basis of the interpretation of the seismic stratigraphy near the site (Shipboard Scientific Party, 1996b), this age must be close to the age of the base of the sediment pile, although the igneous basement was not reached by drilling. Reflectors at Site 987 (Fig. 16) can be traced into the fan depocenter (Fig. 1), providing a chronology for the glacial fan deposit at the

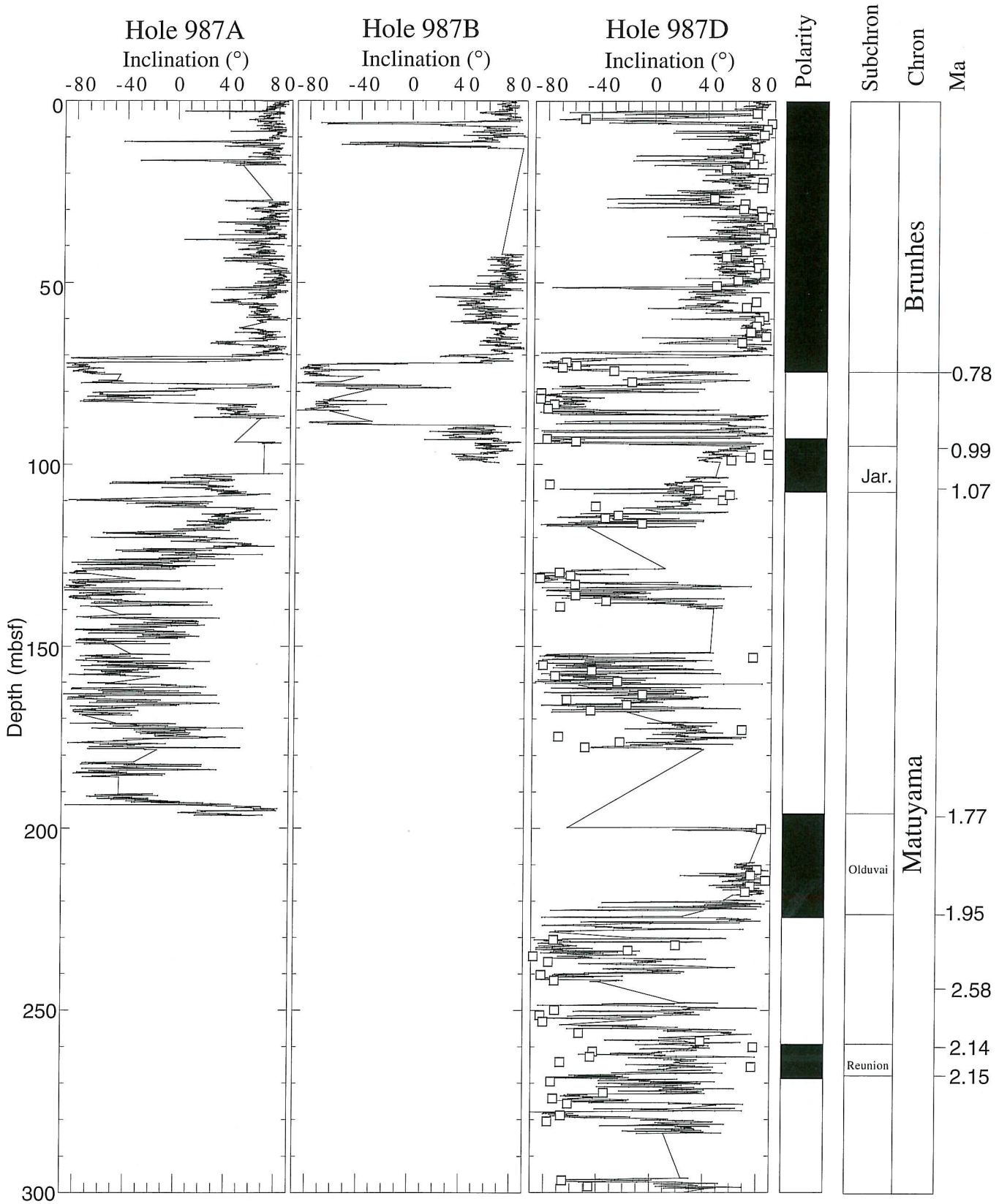

Figure 8. Shipboard (pass-through magnetometer) inclination data after AF demagnetization at peak fields of 25 mT for Holes 987A, 987B, and 987D. Open squares indicate component inclinations determined from discrete (7 cm^3) samples measured postcruise. Component directions computed from orthogonal projections of AF demagnetization data.

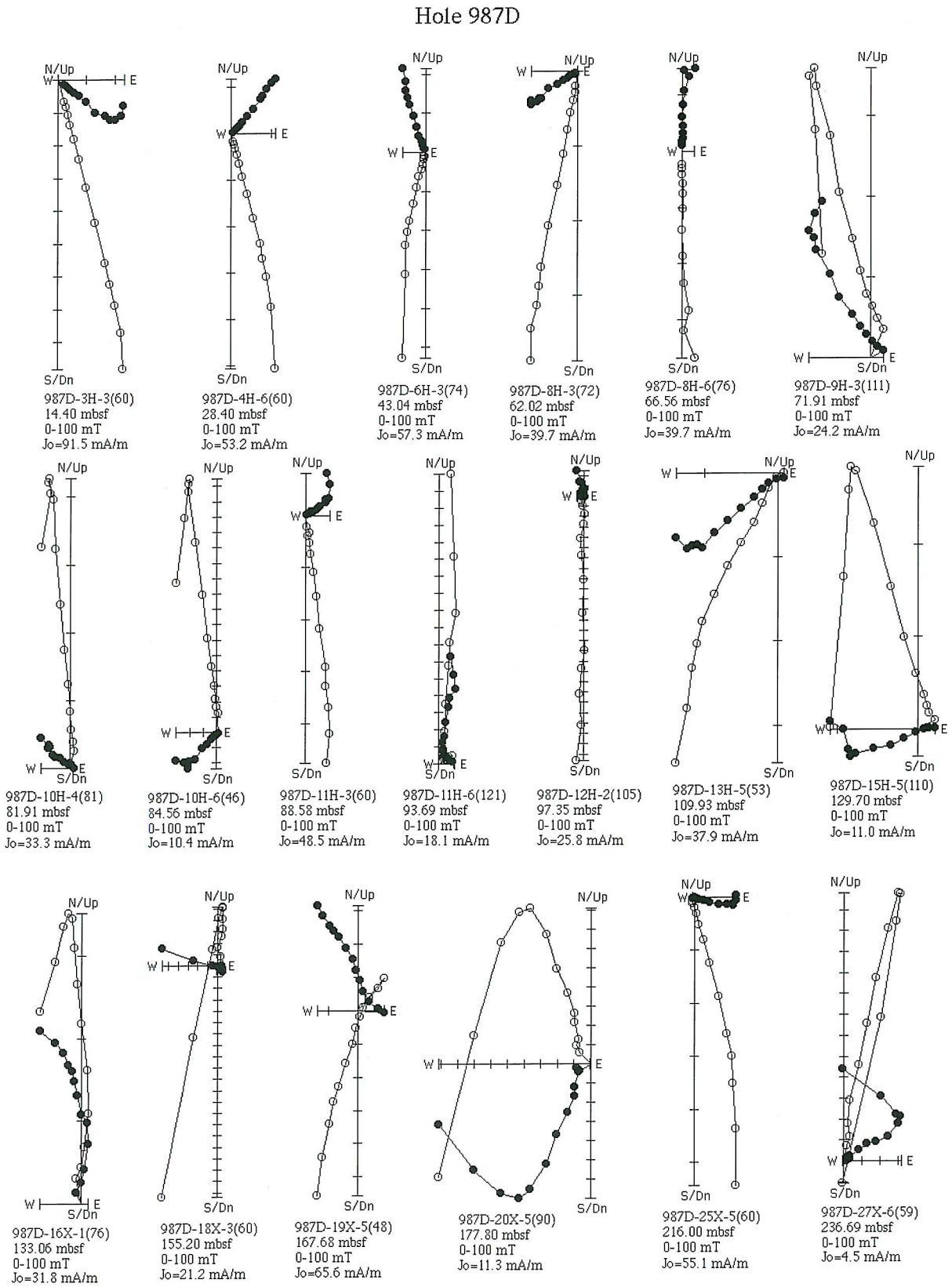

Figure 9. Orthogonal projection of AF demagnetization data from discrete samples in the 0–250 mbsf interval of Hole 987D. Open and solid symbols indicate projection on the vertical and horizontal planes, respectively.

Table 2. Polarity chron boundaries at Site 987.

Event	Age (Ma)	Hole	Depth (mbsf)	Depth (mcd)	Subtracting debris flow 1 Depth (mbsf)	Subtracting debris flow 1 Depth (mcd)	Subtracting debris flow 1 + 2 Depth (mbsf)	Subtracting debris flow 1 + 2 Depth (mcd)
Brunhes/Matuyama	0.78	987A	70	77	70	77	70	77
Brunhes/Matuyama	0.78	987B	72	79	72	79	72	79
Brunhes/Matuyama	0.78	987D	70	79*	70	79*	70	79*
Top, Jaramillo	0.78	987A	84	93	84	93	84	93
Top, Jaramillo	0.99	987B	90	103	90	103	90	103
Top, Jaramillo	0.99	987D	94	106*	94	106*	94	106*
Base, Jaramillo	1.07	987A	103	111	103	111	103	111
Base, Jaramillo	1.07	987D	110	121*	110	121*	110	121*
Top, Olduvai	1.77	987A	195	206	195	206	195	206
Top, Olduvai	1.77	987D	200	210*	200	210*	200	210*
Base, Olduvai	1.95	987D	225	236	225	236	225	236
Reunion	2.14	987D	~263	274	~263	274	~263	274
Mat./Gauss	2.58	987E	370	370	306	306	306	306
Top, Kaena	3.04	987E	438	438	374	374	374	374
Base, Kaena	3.11	987E	448	448	384	384	384	384
Top, Mammoth	3.22	987E	470	470	406	406	406	406
Base, Mammoth	3.33	987E	481	481	417	417	417	417
Gauss/Gilbert	3.58	987E	508	508	444	444	444	444
Top, Cochiti	4.18	987E	547	547	483	483	483	483
Base, Cochiti	4.29	987E	557	557	493	493	493	493
Top, Nunivak	4.48	987E	564	564	500	500	500	500
Base, Nunivak	4.62	987E	573	573	509	509	509	509
Top, C3r	5.23	987E	712	712	648	648	566	566
Base, C3r	5.89	987E	747	747	683	683	601	601
Base, C3An.2n	6.57	987E	793	793	729	729	647	647
Base, C4n.1n	7.43	987E	850	850	786	786	704	704

Note: * = preferred estimate.

mouth of the Scoresby Sund. The oldest occurrence of dropstones off southeast Greenland has been dated at 7 Ma (Larsen et al., 1994). It seems likely that this age marks the onset of significant growth of the Greenland Ice Sheet, although Theide et al. (in press) report ice-rafted debris with a likely Greenland provenance in the deep Norwegian-Greenland Sea since 12–15 Ma.

Sedimentation rates at Site 987 are 50–70 m/m.y. at the base of the section in the 700–850 mbsf interval (Fig. 16). The sedimentation rate increased in the 600-700 mbsf interval, probably in the vicinity of 650 mbsf at the base of lithologic Unit IV (Fig. 16) at ~5 Ma. Lithologic Unit IV is essentially a succession of debris flows. Above lithologic Unit IV, sedimentation rates decreased to 50–100 m/m.y. before increasing again at 2.6 Ma at the base of Unit II, another debris flow unit (Fig. 16). Above the Unit II debris flows, just below the Olduvai Subchron at ~2 Ma, sedimentation rates decrease to 100–150 m/m.y.

The age-depth plot for Site 987 (Fig. 18) illustrates the increases in sedimentation rates associated with the debris flow deposits in the Unit IV (305–369 mbsf) and Unit II (575–657 mbsf) intervals. Subtraction of the debris flow intervals from the section thickness results in more uniform apparent sedimentation rates, providing support for the magnetostratigraphic interpretations.

ACKNOWLEDGMENTS

We thank C. Kissel and C. Laj for logistical support, K. Huang for laboratory assistance, and J. Theide for a review of the manuscript. The paleomagnetic laboratory at Gif-sur-Yvette is supported by CEA and the Centre Nationale de Recherche Scientifique. At the University of Florida, this project was funded by the U.S. Science Support Program, LSCE contribution number 36.

REFERENCES

Andersen, E.S., Solheim, A., and Elverhoi, A., 1994. Development of a glaciated Arctic continental margin: exemplified by the western margin of Svalbard. *In* Thurston, D.K., and Fujita, K. (Eds.), *International Conference on Arctic Margins, Proceedings:* Anchorage, AK (U.S. Dept. of the Interior), MMS 94-0040:155–160.

Berger, W.H., and Jansen, E., 1994. Mid-Pleistocene climate shift: the Nansen connection. *In* Johannessen, O.M., Muensch, R.D., and Overland, J.E. (Eds.), *The Role of the Polar Oceans in Shaping the Global Environment.* Geophys. Monogr., Am. Geophys. Union, 85:295–311.

Berggren, W.A., Hilgen, F.J., Langereis, C.G., Kent, D.V., Obradovich, J.D., Raffi, I., Raymo, M.E., and Shackleton, N.J., 1995a. Late Neogene chronology: new perspectives in high-resolution stratigraphy. *Geol. Soc. Am. Bull.,* 107:1272–1287.

Berggren, W.A., Kent, D.V., Swisher, C.C., III, and Aubry, M.-P., 1995b. A revised Cenozoic geochronology and chronostratigraphy. *In* Berggren, W.A., Kent, D.V., Aubry, M.-P., and Hardenbol, J. (Eds.), *Geochronology, Time Scales and Global Stratigraphic Correlation.* Spec. Publ.—Soc. Econ. Paleontol. Mineral. (Soc. Sediment. Geol.), 54:129–212.

Faleide, J.I., Solheim, A., Fiedler, A., Hjelstuen, B.O., Andersen, E.S., and Vanneste, K., 1996. Late Cenozoic evolution of the western Barents Sea-Svalbard continental margin. *Global Planet. Change,* 12:53–74.

Farrell, J.W., Clemens, S.C., and Gromet, L.P., 1995. Improved chronostratigraphic reference curve of late Neogene seawater $^{87}Sr/^{86}Sr$. *Geology,* 23:403–406.

Fiedler, A., and Faleide, J.I., 1996. Cenozoic sedimentation along the southwestern Barents Sea margin in relation to uplift and erosion of the shelf. *Global Planet. Change,* 12:75–93.

Fronval, T., and Jansen, E., 1996. Late Neogene paleoclimates and paleoceanography in the Iceland-Norweigian Sea: evidence from the Iceland and Vøring Plateaus. *In* Thiede, J., Myhre, A.M., Firth, J.V., Johnson, G.L., and Ruddiman, W.F. (Eds.), *Proc. ODP, Sci. Results,* 151: College Station, TX (Ocean Drilling Program), 455–468.

Hodell, D.A., Mueller, P.A., and Garrido, J.R., 1991. Variations in the strontium isotopic composition of seawater during the Neogene. *Geology,* 19:24–27.

Kirschvink, J.L., 1980. The least-squares line and plane and the analysis of palaeomagnetic data. *Geophys. J. R. Astron. Soc.,* 62:699–718.

Larsen, H.C., 1990. The East Greenland Shelf. *In* Grantz, A., Johnson, G.L., and Sweeney, J.F. (Eds.), *The Arctic Ocean Region.* Geol. Soc. Am., Geol. of North Am. Ser., L:185–210.

Larsen, H.C., Saunders, A.D., Clift, P.D., Beget, J., Wei, W., Spezzaferri, S., and the ODP Leg 152 Scientific Party, 1994. Seven million years of glaciation in Greenland. *Science,* 264:952–955.

Mørk, M.B.E., and Duncan, R.A., 1993. Late Pliocene basaltic volcanism on the Western Barents Shelf margin: implications from petrology and ^{40}Ar-^{39}Ar dating of volcaniclastic debris from a shallow drill core. *Nor. Geol. Tidsskr.,* 73:209–225.

Mudie, P.J., 1989. Palynology and dinocyst biostratigraphy of the late Miocene to Pleistocene, Norwegian Sea: ODP Leg 104, Sites 642–644. *In* Eldholm, O., Thiede, J., Taylor, E., et al., *Proc. ODP, Sci. Results,* 104: College Station, TX (Ocean Drilling Program), 587–610.

Poulsen, N.E., Manum, S.B., Williams, G.L., and Ellegaard, M., 1996. Tertiary dinoflagellate biostratigraphy of Sites 907, 908, and 909 in Norwegian-Greenland Sea. *In* Thiede, J., Myhre, A.M., Firth, J.V., Johnson, G.L., and Ruddiman, W.F. (Eds.), *Proc. ODP, Sci. Results,* 151: College Station, TX (Ocean Drilling Program), 255–287.

Pozzi, J.-P., Barthés, V., Thibal, J., Pocachard, J., Lim, M., Thomas, T., and Pages, G., 1993. Downhole magnetostratigraphy in sediments: comparison with the paleomagnetism of a core. *J. Geophys. Res.,* 98:7939–7957.

Shipboard Scientific Party, 1996a. Site 986. *In* Jansen, E., Raymo, M.E., Blum, P., et al., *Proc. ODP, Init. Repts.,* 162: College Station, TX (Ocean Drilling Program), 287–343.

————, 1996b. Site 987. *In* Jansen, E., Raymo, M.E., Blum, P., et al., *Proc. ODP, Init. Repts.*, 162: College Station, TX (Ocean Drilling Program), 345–387.

Solheim, A., Andersen, E.S., Elverhoi, A., and Fiedler, A., 1996. Late Cenozoic depositional history of the western Svalbard continental shelf, controlled by subsidence and climate. *Global Planet. Change,* 12:135–148.

Spiegler, D., and Jansen, E., 1989. Planktonic foraminifer biostratigraphy of Norwegian Sea sediments: ODP Leg 104. *In* Eldholm, O., Thiede, J., Taylor, E., et al., *Proc. ODP, Sci. Results,* 104: College Station, TX (Ocean Drilling Program), 681–696.

Talwani, M., and Eldholm, O., 1977. Evolution of the Norwegian-Greenland Sea. *Geol. Soc. Am. Bull.,* 88:969–999.

Theide, J., Winkler, A., Wolf-Welling, T., Eldholm, O., Myhre, A.M., Baumann, K.H., Heinrich, R., and Stein, R., 1998. Late Cenozoic history of the polar North Atlantic margins: results from ocean drilling. *Quat. Sci. Rev.,* 17:185–208.

Date of initial receipt: 10 September 1997
Date of acceptance: 15 April 1998
Ms 162SR-008

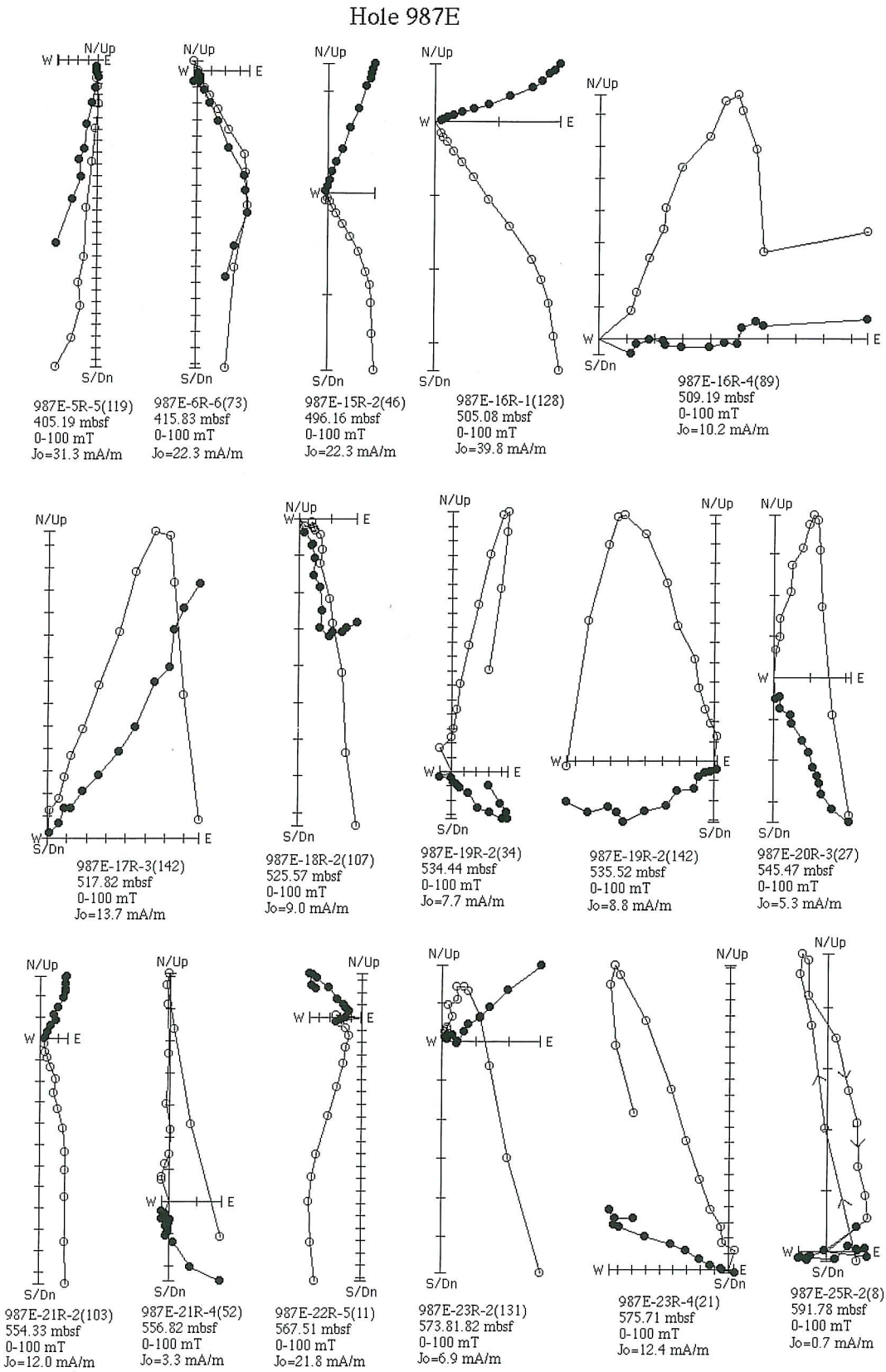

Figure 10. Orthogonal projection of AF demagnetization data from discrete samples in the 400–600 mbsf interval of Hole 987E. Open and solid symbols indicate projection on the vertical and horizontal planes, respectively.

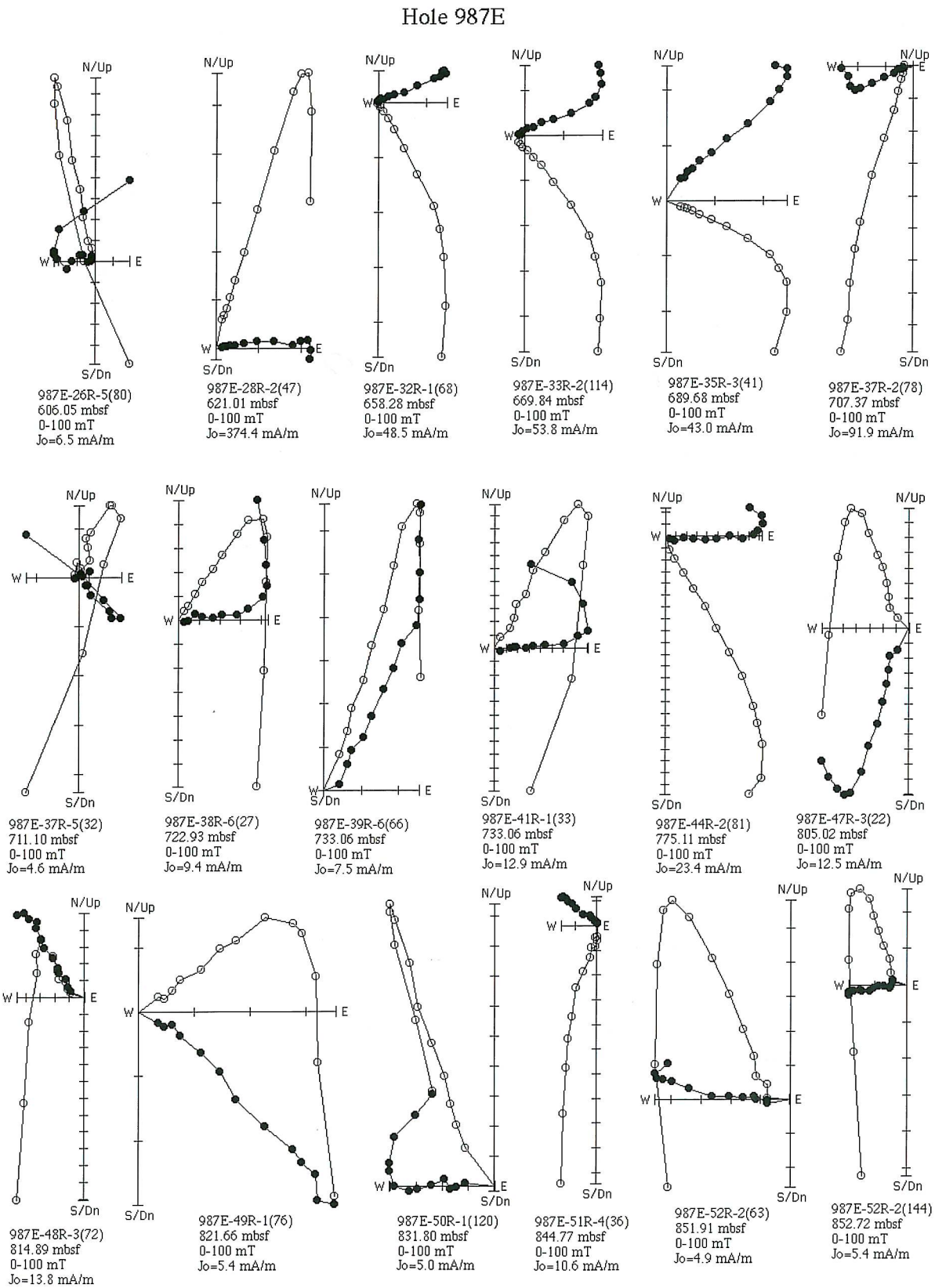

Figure 11. Orthogonal projection of AF demagnetization data from discrete samples in the 600–900 mbsf interval of Hole 987E. Open and solid symbols indicate projection on the vertical and horizontal planes, respectively.

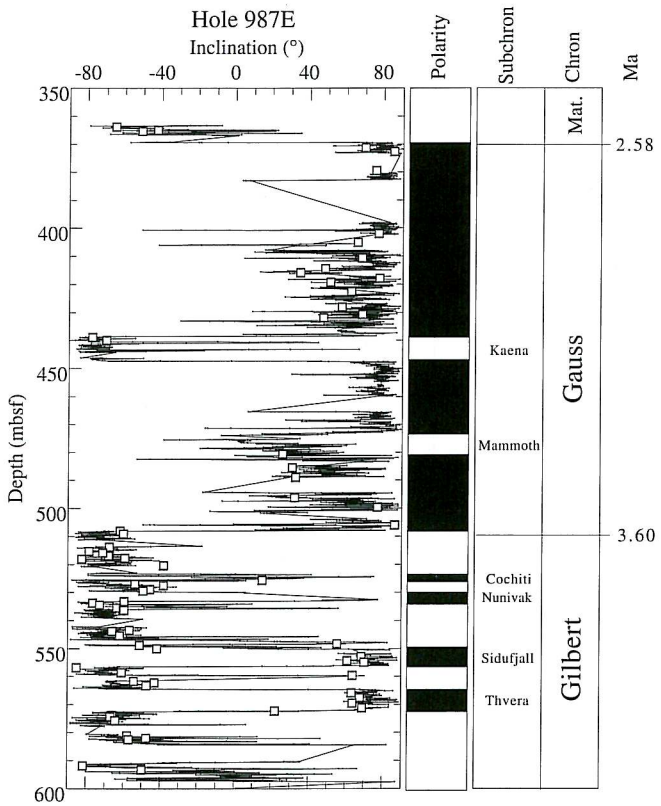

Figure 12. Shipboard (pass-through magnetometer) inclination data after AF demagnetization at peak fields of 25 mT for Hole 987E in the 350–600 mbsf interval. Open squares indicate component inclinations determined from discrete (7 cm^3) samples measured postcruise. Component directions computed from orthogonal projections of AF demagnetization data.

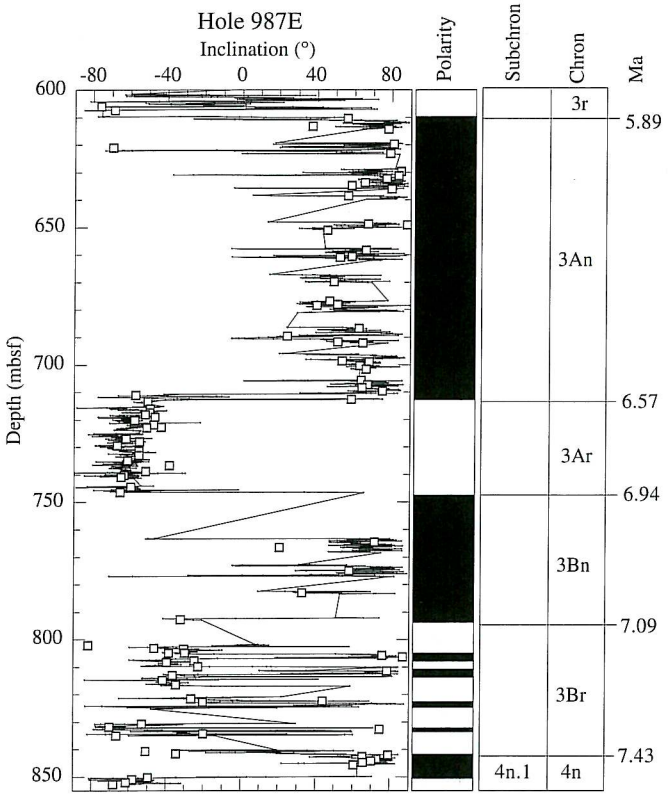

Figure 13. Shipboard (pass-through magnetometer) inclination data after AF demagnetization at peak fields of 25 mT for Hole 987E in the 600–860 mbsf interval. Open squares indicate component inclinations determined from discrete (7 cm^3) samples measured postcruise. Component directions computed from orthogonal projections of AF demagnetization data.

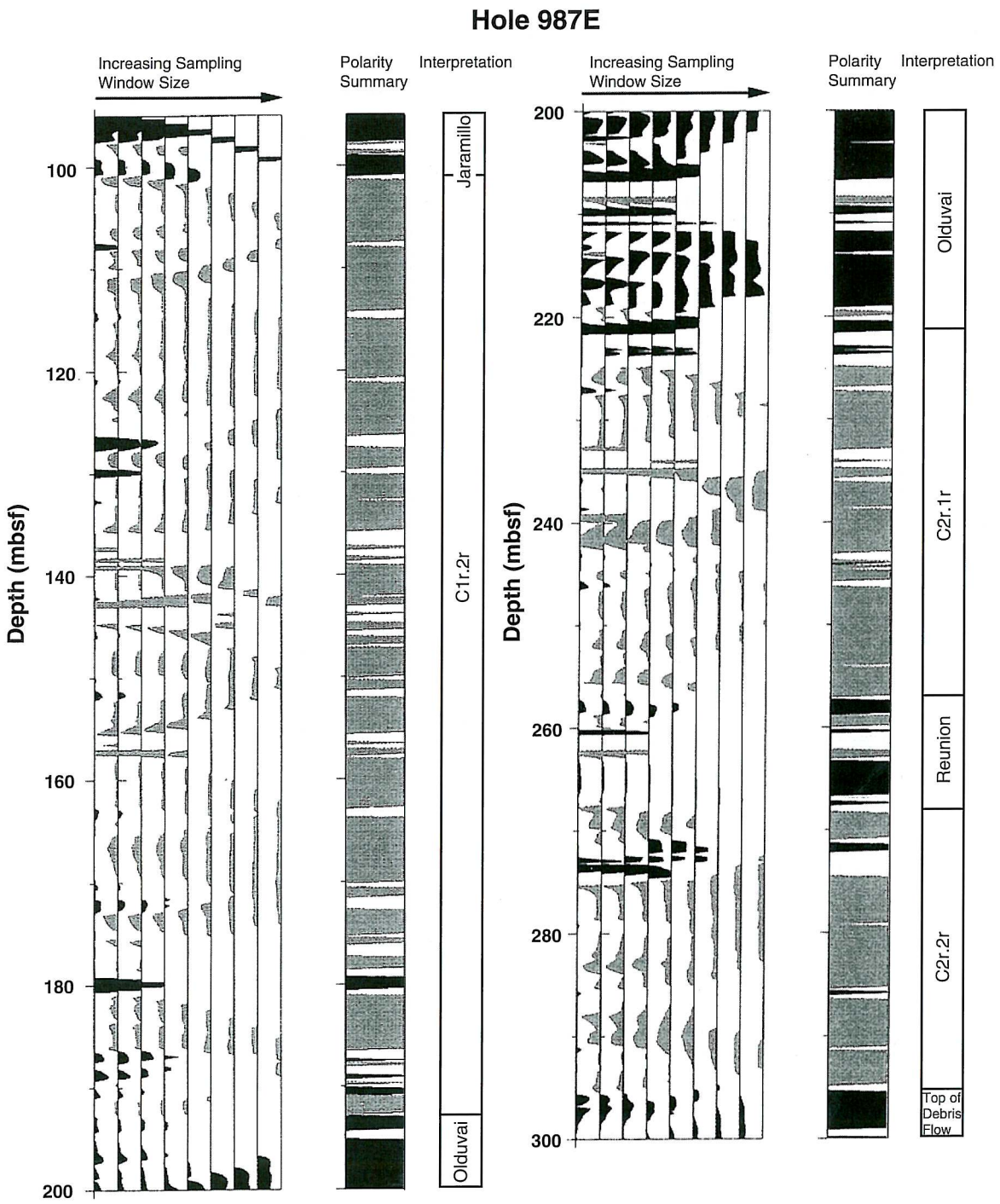

Figure 14. GHMT wireline logs at Hole 987E. Positive correlations of susceptibility and remanence imply normal polarities (black), and negative correlations imply reverse polarity (gray). The correlations were assessed in a number of sampling windows, increasing from ~1 to ~25 m from left to right. Only windows with lengths from 1.5 to ~16 m were used to create the polarity summary column based on a minimum correlation coefficient of 0.5.

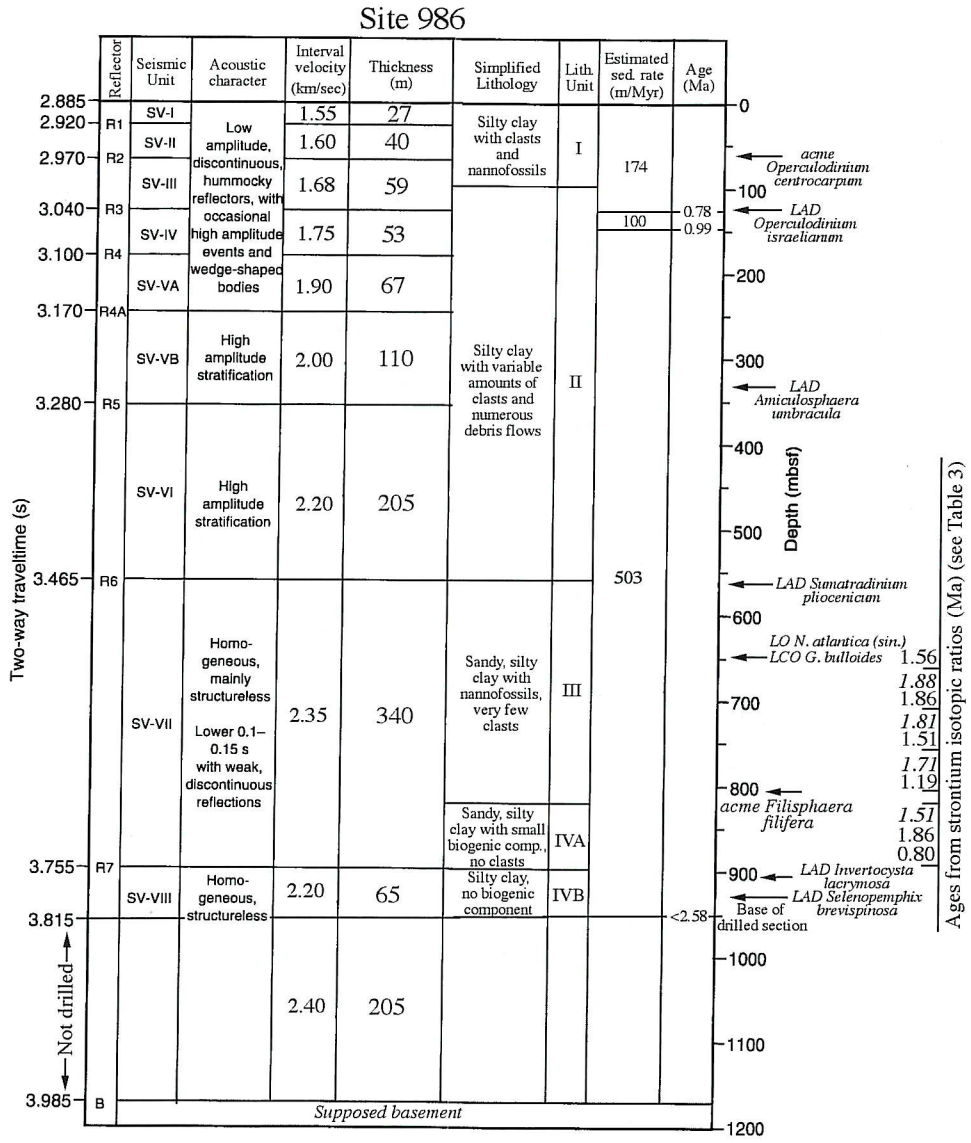

Figure 15. Site 986 seismic reflectors and seismic units (Shipboard Scientific Party, 1996a) compared to core lithology and magnetostratigraphically deduced ages (see Table 1). Sedimentation rates between age-control points and dinoflagellate events are indicated. Ages deduced from strontium isotopic ratios are derived from benthic (italics) and planktic species (see Table 3).

Table 3. Strontium isotope data, Hole 986D.

Depth (mbsf)	Planktic/Benthic	$^{87}Sr/^{86}Sr$	Age (Ma)
668.42	P	0.709086	1.56
714.92	P	0.709068	1.86
714.92	B	0.709067	1.88
760.82	P	0.709089	1.51
760.82	B	0.709071	1.81
804.42	P	0.709108	1.19
804.42	B	0.709077	1.71
820.02	P	0.709089	1.51
820.02	B	0.709068	1.86
892.42	P	0.709131	0.80

Notes: P = planktic, B = benthic. Ages from Hodell et al. (1991).

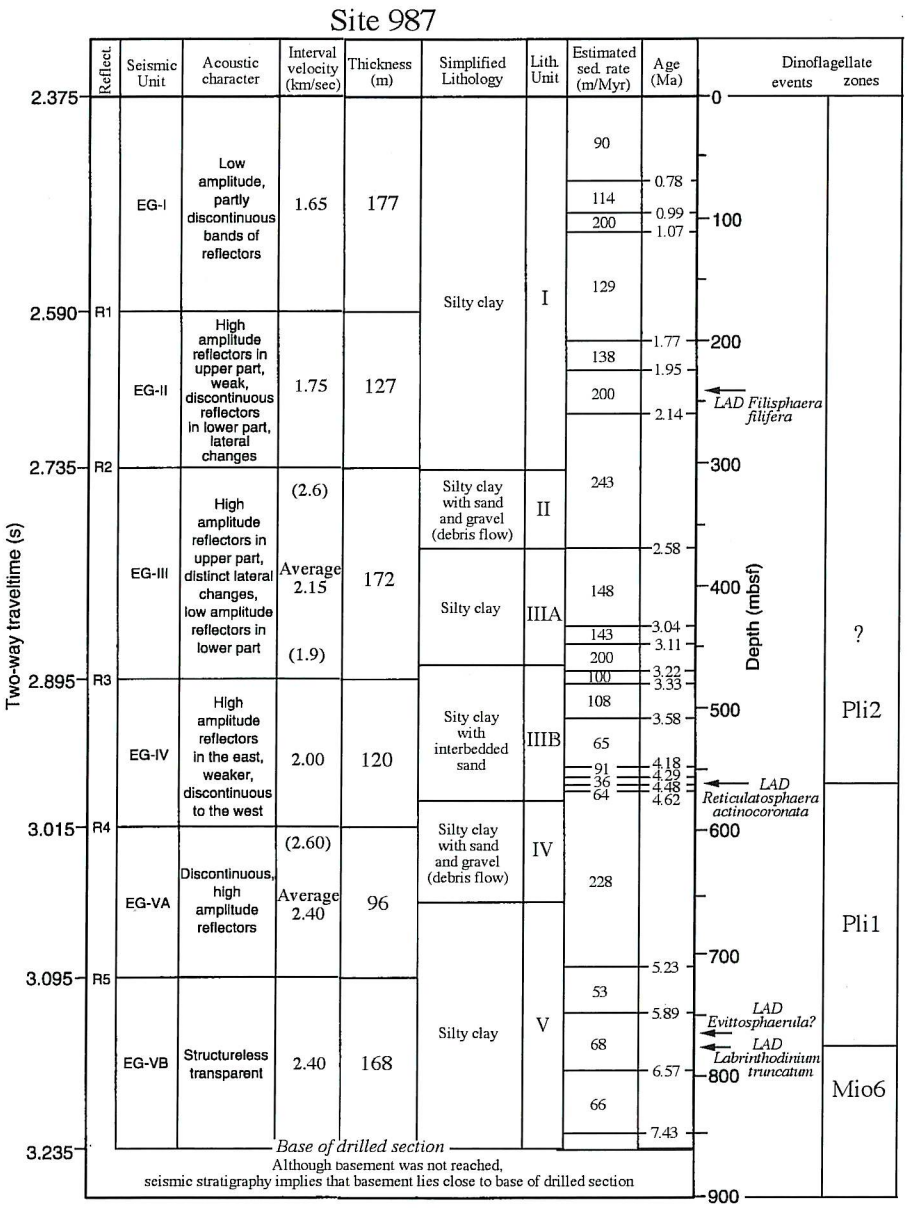

Figure 16. Site 987 seismic reflectors and seismic units (Shipboard Scientific Party, 1996b) compared to core lithology and magnetostratigraphically deduced ages (see Table 2). Sedimentation rates between age-control points are indicated. Dinoflagellate events and zones (Poulsen et al., 1996) are shown.

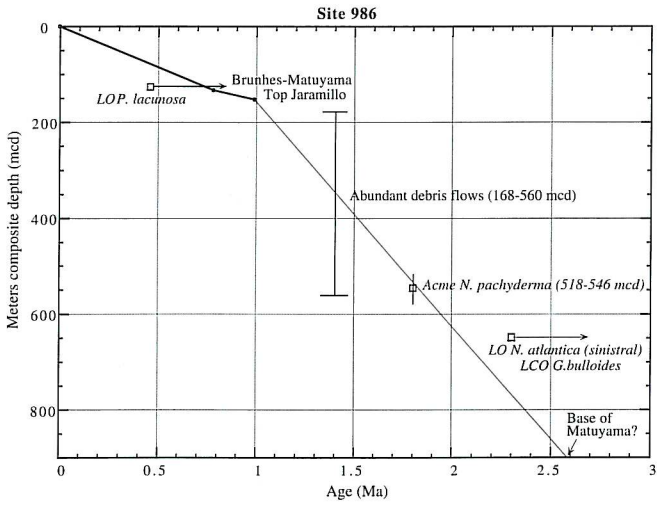

Figure 17. Site 986 age-depth plot based on magnetostratigraphic interpretation. High sedimentation rates are apparent in the interval characterized by abundant debris flows. The age model is inconsistent with the occurrence of *N. atlantica* (sinistral) in the 647–955 interval, which would imply that this entire interval is older than 2.3 Ma.

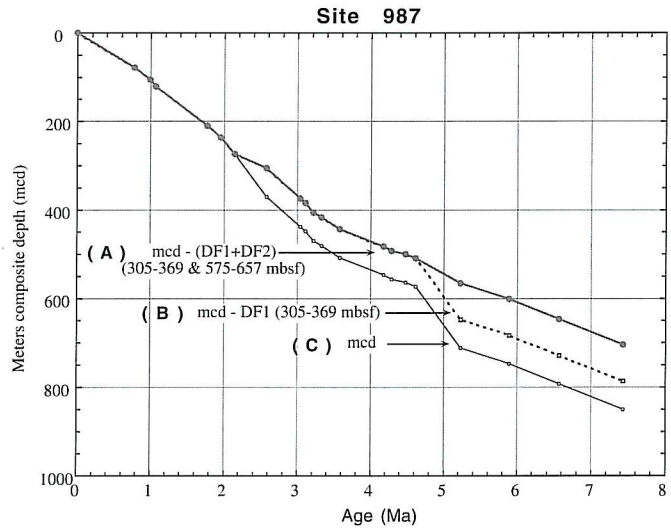

Figure 18. Site 987 age-depth plots based on magnetostratigraphic interpretation. The composite section at Site 987 does not extend below 368 mcd; therefore, mcd and mbsf are taken as equivalent below this depth. Debris Flow 1 (DF1) was detected in the IDPH resistivity log (Fig. 2B) in the 305–369 mbsf depth interval of Hole 987E (equivalent to lithologic Unit 2 and ~316–379 mcd). **A.** Age-depth plot after subtraction of two major debris flow intervals (in the 305–369 and 575–657 mbsf intervals). **B.** Age-depth plot after subtracting one of the debris flow intervals (305–369 mbsf interval). **C.** Age-depth plot without subtracting debris flows.